How to cite: *Angew. Chem. Int. Ed.* **2022,** *61,* e202210224
International Edition: doi.org/10.1002/anie.202210224
German Edition: doi.org/10.1002/ange.202210224

Analytical Methods | Hot Paper

Direct Acquisition of the Gap Height of Biological Tissue-Electronic Chemical Sensor Interfaces

Xin-Wei Zhang, Amir Hatamie, and Andrew G. Ewing**

Abstract: Interfacing biological tissues with electronic sensors offers the exciting opportunity to accurately investigate multiple biological processes. Accurate signal collection and application are the foundation of these measurements, but a long-term issue is the signal distortion resulting from the interface gap. The height of the gap is the key characteristic needed to evaluate or model the distortion, but it is difficult to measure. By integrating a pair of nanopores at the electronic sensor plane and measuring the ion conductance between them, we developed a versatile and straightforward strategy to realize the direct cooperative evaluation of the gap height during exocytotic release from adrenal gland tissues. The signaling distortion of this gap has been theoretically evaluated and shows almost no influence on the amperometric recording of exocytosis in a classic "semi-artificial synapse" configuration. This strategy should benefit research concerning various bio/chemical/machine interfaces.

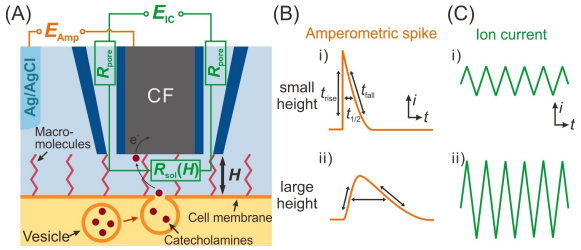

Figure 1. A) Schematic of the ion conductance-amperometric (IC-Amp) measurement. For the amperometric (Amp) recording, a constant potential ($E_{Amp} = +700$ mV vs. Ag/AgCl) was applied to the CFME to record the exocytotic catecholamines. For the ion conductance (IC) measurement, a triangle wave potential (E_{IC}, amplitude: 100 mV, scan rate: 1 V/s) was applied to the two nanopores neighboring the CFME. The resistance of the IC measurement circuit mainly includes the resistance of the solution within the cell to electrode gap ($R_{sol}(H)$) and inside the two nanopores (R_{pore}). The IC-Amp sensor was placed on a cell and a gap (its height is indicated as H) was formed because of the macro-molecules on the cell membrane. B) Schematic of an amperometric spike at a small H (i) vs. large H (ii). C) Schematic of the ion current through the nanopores at a small H (i) vs. large H (ii).

Interfacing biological tissues/cells with electronic sensors offers the exciting opportunity to accurately investigate multiple biological processes.[1] For decades, the "semi-artificial synapse"[2] (shown as "Amp circuit" in Figure 1A) has been used as a classic and mass-applied bio-machine interface structure. This has been used to investigate exocytosis and a wide scope of related biological processes, like neuronal signaling transduction[3] and endocrine regulation.[4] When exocytosis is triggered, the released catecholamines diffuse from the pre-synaptic side, are electrooxidized at the carbon fiber micro-disk electrode (CFME, as the artificial post-synapse), and generate a spike-shaped signal through an amperometric recording (Figure 1Bi).[2a]

Accurate signal collection is fundamental to the investigation of biological processes focusing on tissue/cells-electric sensor interfaces. However, the interface gap may distort the signal transduction. For the "semi-artificial synapse" configuration, the dimension of the gap within interface and its distortion effects on the recorded signals have been repeatedly questioned and discussed.[5] The Wightman group was the earliest to report peak distortion (Figure 1Bii) when a CFME was positioned with a set distance from the cell.[5d,6] This alteration of the spike shape reflects the delay of mass transfer when a species diffuses across the gap, which can be likened to a kind of digital filtering, called "diffusional filtering" (also "diffusion broadening"[5d] or "diffusion distortion"[2a,5c]). Furthermore, this filtering phenomenon of gaps widely exists in any bio-machine interface, and more specific investigations are urgently required. An exact model of the diffusional filtering in the electrode-cell interface is still absent, due primarily to the difficulty in modeling the gap[2a] whose height (see H in Figure 1A) has only been hypothesized[7] or theoretically estimated.[5a,8]

To better understand the interface gap within an artificial synapse, some insights have been provided by scanning ion conductance microscopy (SICM), which was used to image the topography of the biological samples.[9] By

[*] Dr. X.-W. Zhang
College of Chemistry and Molecular Sciences, Wuhan University
430072 Wuhan (China)
E-mail: xinweizhang@whu.edu.cn
Dr. X.-W. Zhang, Dr. A. Hatamie, Prof. Dr. A. G. Ewing
Department of Chemistry and Molecular Biology, University of Gothenburg
41296 Gothenburg (Sweden)
E-mail: andrew.ewing@chem.gu.se

quantifying the ion current, the height between the probe and the sample surface can be measured. In particular, double pipette-SICM[10] provides a relatively robust strategy to overcome the instability of single pipette-SICM when it is pressed on a soft biological matrix. However, fabrication instability and clogging of double-pipettes might lead the height measurement to be unreliable, and its different morphology compared to the actual planar electric sensors make it difficult to reflect the real height between tissue/cells and electric sensors.

In this paper, we developed a new strategy to integrate ion conductance measurements into the classical configuration of the semi-artificial synapse. This provides a direct analysis of the gap between the cell and the electrode while exocytosis is recorded at the same sensor. The filtering characteristics of the gap with the measured height were numerically analyzed, and its diffusional filtering effect on the exocytotic signals was quantitatively evaluated.

To realize the in situ measurement of ion conductance, we designed an ion conductance-amperometric (IC-Amp) sensor by integrating two tiny nanopores neighboring the traditional disk electrode and sharing the same plane (schematic in Figure 1A). Theoretically, the ion current and conductance (G_{sol}) will vary with the gap height (H) between the probe and the sample surface (schematic in Figure 1C). The $G_{sol}(H)$ can be calculated as follows:

$$G_{sol}(H) = \frac{1}{R_{total}(H)} = \frac{1}{R_{total}(H) - R_{pore}} \approx \frac{1}{R_{total}(H) - R_{total}(\infty)} = \frac{1}{E_{IC}/I(H) - E_{IC}/I(\infty)} \quad (1)$$

where the $R_{sol}(H)$ is the resistance of the solution within the gap, the $R_{total}(H)$ is the total resistance of the IC circuit which can be obtained by dividing the applied potential (E_{IC}) by the measured ion current ($I(H)$), and R_{pore} is the solution resistance of the nanopores which can be measured as $R_{total}(\infty)$ (i.e. the total resistance of IC circuit when $H \to \infty$). After establishing the value of R_{pore} in the R_{total}(H), we calculate $G_{sol}(H)$ by Equation (1). However, $G_{sol}(H)$ is not only related to the solution geometry outside the two nanopores, but also the solution conductivity (expressed as the $G_{sol}(H) \propto$ the solution conductivity). To diminish the influence of the variation in solution conductibility for different experiments by normalization, we adopted a term for the relative $G_{sol}(H)$ ($= G_{sol}(H)/G_{sol}(H \to \infty)$), instead of the $G_{sol}(H)$, to measure the H in the following experiments. The $G_{sol}(H \to \infty)$ is the conductance of the solution outside the nanopores when the nanopores are very far away from the substrate, which is constant for an IC-Amp sensor with fixed solution conductivity (see calculation details in Supporting Information).

The IC-Amp sensor was fabricated by heat-pulling a 7-barrel glass capillary with a carbon fiber in the center barrel, and then beveling it to generate a sensor plane including the center elliptic CFME and six surrounding nanopores (see Figure 2 and Supporting Information). Only the pair of nanopores located on the short axis of the ellipse were adopted for the IC measurement, because the other 4 pores were sometimes broken or defective resulting from the vibration during the beveling. This fabrication allows CFME detection of release with the introduction of the nanopores on either side without a large change in the CFME structure. Moreover, although the pore sizes or positions may vary over a range of several times because of possible instability of fabrication, the IC measurement using the relative G_{sol}-(H) as output was still highly robust and verified by theoretical simulation (simulation details of IC measurement in Supporting Information and Figure S1–3).

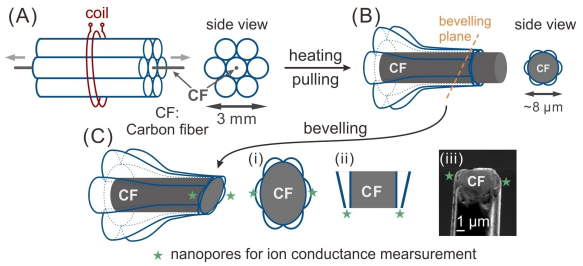

Figure 2. Schematic of the fabrication of the IC-Amp sensor. A) A 7-barrel glass capillary with a carbon fiber (d: 5 μm) in the center barrel was heated and pulled to a small tip; B) the carbon fiber was wrapped by the glass wall, whereas the 6 surrounding barrels were crescent shaped; C) after beveling, the probe tip was planar with the center elliptical CFME and 6 surrounding nanopores. (i) the view of the beveled plane, (ii) cross-sectional view and (iii) a scanning electron microscopy image of the IC-Amp sensor. The two nanopores used for IC measurement are labeled by asterisks.

The IC-Amp sensor was experimentally calibrated by constructing a height-controlled gap between the sensor and the substrate (schematic in Figure 3A). After filling the nanopores with an electrolyte solution and applying E_{IC}, the IC-Amp sensor was placed onto a series of polydimethylsiloxane (PDMS) sheets[11] with small pillars of different heights (H = 90, 380, 520, 770, 1150 nm, diameter 500 nm, circle center distance 1500 nm, see examples in Figure 3B and the fabrication in the Supporting Information) by use of a micro-manipulator. These pillars on the PDMS sheets mimic the cellular membrane macromolecules, which create space between the soft cell membrane and the sensor. The approach of the sensor tip was observed by monitoring the decline of the ion current amplitude (Figure 3C). The decreased ion current amplitude was converted to the relative $G_{sol}(H)$ [Eq. (1)], and the relationship between relative $G_{sol}(H)$ and the gap heights made by the pillars was constructed and almost matches the simulation (Figure 3D, simulation configuration is shown in the Supporting Information).

The medulla cells of bovine adrenal glands are often used in the analysis of exocytosis.[12] To simulate the bio-machine interface that is constructed between an electrode and tissue, instead of a single cell, we applied the IC-Amp sensor on slices of the fresh bovine adrenal medulla (see the slice preparation in the Supporting Information) and carried out in situ measurements of the gap height and exocytotic recording at the same sensor (Figure 1A). To avoid interference between measurements, they were carried out in

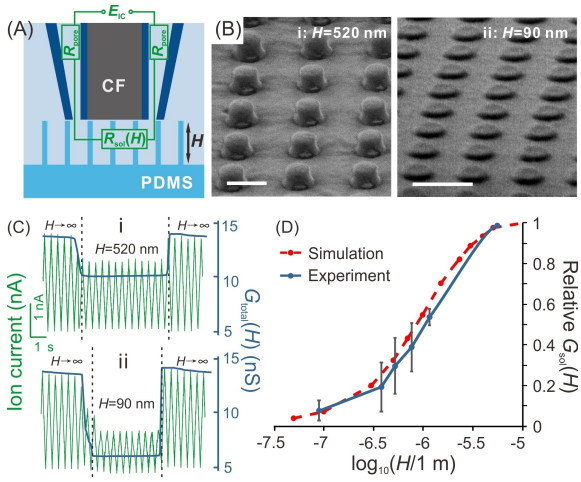

Figure 3. A) Schematic of the IC measurement on PDMS sheets. E_{IC}: triangle wave, amplitude: 100 mV, scan rate: 1 V s^{-1}. B) Scanning electron microscopy images of the PDMS sheets. Scale bar: 1 μm. C) Ion current ($I(H)$) and calculated ion conductance of the IC circuit ($G_{total}(H) = I(H)/E_{IC}$). The variation of ion current amplitude and $G_{total}(H)$ reflects the IC change when the sensor is moved from far ($H \to \infty$) to contacting the sheets ($H = 520$ nm (i) or 90 nm (ii)) and then moved back ($H \to \infty$). D) Experimental and simulated relative $G_{sol}(H) - H$ curves for this calibration experiment. The error bars present the standard deviations of relative $G_{sol}(H)$ at respective H ($n = 5$).

sequence. The IC measurement was first conducted in a similar manner to the calibration experiments but the PDMS sheets in Figure 3A were replaced by the gland slices. Similarly to the IC change in calibration experiments shown in Figure 3C, the recorded ion current amplitude rapidly decreased after the IC-Amp sensor contacted the surface of the glands (Figure 4A). The gap height was calculated by examining the relative $G_{sol}(H) - H$ standard curve (Figure 3D). After the IC measurement, without moving the sensor, the E_{IC} was stopped and E_{Amp} was then applied to the CFME for amperometric recording of the exocytosis events (Figure 4B). The exocytosis in these systems is spontaneous but depends on the activity of glands, so usually glands stored for too long time (>8 h) give few intense exocytosis events (see the amperometric trace of a slice of less active gland in Figure S4).

Data for IC and amperometric measurements (6 IC traces and 779 amperometric spikes, each spike representing one exocytosis event) from five tissue slices were analyzed. The relative $G_{sol}(H)$ was found to be 0.10 ± 0.03 (mean ± SD), and the H was 134 ± 20 nm (mean ± SD) which is in the same range as previous estimations.[8b,13] This exact gap height provides the possibility to construct accurate numerical models for diffusion in the gap of the artificial synapse.

We then simulated various spike shapes at different gap heights (range from 1 to 500 nm; see Supporting Information and Figure S5A) by a finite element method, referenced to a series of previous works.[8b,14] The original spike, i.e. the current measured at the exocytotic pore site can be calculated by integrating the normal flux of catecholamines across the exocytotic pore and transforming the flux into current by use of Faraday's law, as described by,

$$I_{exo} = \oint\!\!\oint_{S_{pore}} Z_e F J_{exo} dS \tag{2}$$

where the z_e is the charge transfer number, which equals 2 in this work; F is the Faraday constant, 96 500 C mol^{-1}, J_{exo} is the flux density of catecholamine across the exocytotic pore, S_{pore} is the pore area.

When the electrode surface was placed at a gap height away from the exocytotic pore, the free diffusion of catecholamine within the gap causes the simultaneously released molecules to reach the electrode surface at different times. Based on Engstrom's analysis,[5c] and after transforming the flux to be current by Faraday's law, this phenomenon can be expressed as a convolution equation,

$$I(t) = I_{exo}(t) * f(t) \tag{3}$$

where $I(t)$ is the current spike collected by the electrode placed at a given gap height H, $f(t)$ is the "impulse response function" of this convolution system and quantitatively reflects the broadening effects.

By Fourier transformation, the $f(t)$ at each gap height can be further transformed to a frequency domain function which is analogous to the frequency response function of a low-pass filter (see the characteristic curves in Figure S5B). The estimated cut-off frequency, i.e. the frequency at which the magnitude response is 3 dB lower than the value at 0 Hz, of the low-pass filter corresponding to the 134-nm-high gap is about 1.7 kHz and its time constant (τ_f) is ≈0.29 ms (Figure S5C). This τ_f is much smaller than the rise time of the recorded amperometric spikes (t_{rise}: 2.46 ± 0.15 ms (median ± SEM), 25 %-75 % of the amplitude). So, based on these data, we can write the following equation for the rise time of a recorded spike as a relationship between the rise time of original exocytotic spike and the time constant of low-pass filter,[15]

$$t_{rise} \approx \sqrt{t_{exo}^2 + \tau_f^2} \tag{4}$$

here the t_{exo} is the rise time of the original exocytotic spike. The simulated spike for $H = 1$ nm was seen as the original exocytotic spike because of the extremely small height, and the others are those with rise times that can be calculated according to Equation (4). The influence of the low-pass filter for the rising part of spike is essentially negligible,

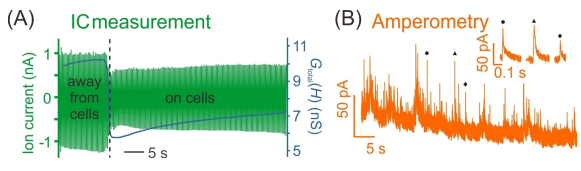

Figure 4. Representative IC measurement trace (A) and amperometric trace (B) for experiments on bovine adrenal gland slices. Three spikes were amplified as the inset in (B).

since the weight of τ_f for t_{rise} is only about 1.4 % from τ_f^2/t_{rise}^2 based on Equation (4). This equation can also be used to calculate the falling part of the spike whose time (t_{fall}: 11 ± 0.59 ms (median ± SEM), 75 %-25 % of the amplitude) is much longer than the rising part of the spike, whereas the weight of τ_f for t_{fall} is 0.07 % and thus its influence can be ignored as well.

In conclusion, to evaluate the signal distortion owing to the gap between the biological tissue-electric sensor interface, and related to gaps between membranes of cells and tissues, we have developed a versatile strategy to measure the gap height by measuring the ion conductance variation with the tissue-sensor gap height for parallel amperometric and ion conducting nanoelectrodes. Using a bovine adrenal gland slice and this parallel sensor interface, direct cooperative measurement of the gap height and exocytotic release at the same sensor can be used to address a long-term question of the influence of diffusional filtering on the exocytotic spike. This strategy shows excellent robustness and should be applicable to gaps in tissues and between cells and will also benefit research on various bio/machine interfaces, like deep-brain stimulation, brain/machine interfaces, pacemakers and other implanted sensors.

Acknowledgements

This work was supported by the European Research Council (ERC Advanced Grant Project No 787534 NanoBioNext), Knut and Alice Wallenberg Foundation, and the Swedish Research Council (VR Grant No 2017-04366). The authors acknowledge Dr. Gan Wang for his work on the nanofabrication, characterization of the PDMS sheets and beneficial suggestions on this manuscript. The authors acknowledge Myfab Chalmers where the nanofabrication for this work was performed at. The authors acknowledge Dalsjöfors Kött AB (Dalsjöfors, Sweden) for donation of bovine adrenal glands.

Conflict of Interest

The authors declare no conflict of interest.

Data Availability Statement

The data that support the findings of this study are available from the corresponding author upon reasonable request.

Keywords: Biological Tissues · Diffusional Filtering · Exocytosis · Interfaces · Ion Conductance

[1] a) R. Feiner, T. Dvir, *Nat. Rev. Mater.* **2018**, *3*, 17076; b) M. D. Serruya, N. G. Hatsopoulos, L. Paninski, M. R. Fellows, J. P. Donoghue, *Nature* **2002**, *416*, 141–142.

[2] a) C. Amatore, S. Arbault, M. Guille, F. Lemaitre, *Chem. Rev.* **2008**, *108*, 2585–2621; b) C. Amatore, S. Arbault, N. Sojic, M. Vuillaume, *Ultramicroelectrodes: Their Use in Semi-Artificial Synapses, Novel Trends in Electroorganic Synthesis*, Springer, Berlin, **1998**.

[3] a) M. L. Huffman, B. J. Venton, *Analyst* **2009**, *134*, 18–24; b) R. H. Westerink, *Neurotoxicology* **2004**, *25*, 461–470.

[4] a) J. M. Finnegan, K. Pihel, P. S. Cahill, L. Huang, S. E. Zerby, A. G. Ewing, R. T. Kennedy, R. M. Wightman, *J. Neurochem.* **1996**, *66*, 1914–1923; b) A. Hatamie, L. Ren, H. Dou, N. R. Gandasi, P. Rorsman, A. Ewing, *Angew. Chem. Int. Ed.* **2021**, *60*, 7593–7596; *Angew. Chem.* **2021**, *133*, 7671–7674.

[5] a) A. S. Cans, N. Wittenberg, R. Karlsson, L. Sombers, M. Karlsson, O. Orwar, A. Ewing, *Proc. Natl. Acad. Sci. USA* **2003**, *100*, 400–404; b) A. S. Cans, N. Wittenberg, D. Eves, R. Karlsson, A. Karlsson, O. Orwar, A. Ewing, *Anal. Chem.* **2003**, *75*, 4168–4175; c) R. C. Engstrom, R. M. Wightman, E. W. Kristensen, *Anal. Chem.* **1988**, *60*, 652–656; d) T. J. Schroeder, J. A. Jankowski, K. T. Kawagoe, R. M. Wightman, C. Lefrou, C. Amatore, *Anal. Chem.* **1992**, *64*, 3077–3083.

[6] a) J. A. Jankowski, T. J. Schroeder, E. L. Ciolkowski, R. M. Wightman, *J. Biol. Chem.* **1993**, *268*, 14694–14700; b) K. T. Kawagoe, J. A. Jankowski, R. M. Wightman, *Anal. Chem.* **1991**, *63*, 1589–1594.

[7] a) Y. Bouret, M. Guille-Collignon, F. Lemaitre, *Anal. Bioanal. Chem.* **2021**, *413*, 6769–6776; b) R. Trouillon, A. G. Ewing, *Anal. Chem.* **2013**, *85*, 4822–4828.

[8] a) B. B. Anderson, S. E. Zerby, A. G. Ewing, *J. Neurosci. Methods* **1999**, *88*, 163–170; b) C. Gu, X. Zhang, A. G. Ewing, *Anal. Chem.* **2020**, *92*, 10268–10273; c) I. Hafez, K. Kisler, K. Berberian, G. Dernick, V. Valero, M. G. Yong, H. G. Craighead, M. Lindau, *Proc. Natl. Acad. Sci. USA* **2005**, *102*, 13879–13884.

[9] a) F. Anariba, J. H. Anh, G. Jung, N. Cho, S. Cho, *Mod. Phys. Lett. B* **2012**, *26*, 1130003; b) P. Happel, D. Thatenhorst, I. D. Dietzel, *Sensors* **2012**, *12*, 14983–15008; c) B. C. Liu, X. Y. Lu, X. Song, K. Y. Lei, A. A. Alli, H. F. Bao, D. C. Eaton, H. P. Ma, *Front. Plant Physiol.* **2012**, *3*, 483.

[10] a) N. Ebejer, M. Schnippering, A. W. Colburn, M. A. Edwards, P. R. Unwin, *Anal. Chem.* **2010**, *82*, 9141–9145; b) M. E. Snowden, A. G. Güell, S. C. S. Lai, K. McKelvey, N. Ebejer, M. A. O. Connell, A. W. Colburn, P. R. Unwin, *Anal. Chem.* **2012**, *84*, 2483–2491.

[11] C. Con, B. Cui, *Nanoscale Res. Lett.* **2013**, *8*, 394.

[12] a) M. E. Graham, R. J. Fisher, R. D. Burgoyne, *Biochimie* **2000**, *82*, 469–479; b) D. J. Leszczyszyn, J. A. Jankowski, O. H. Viveros, E. J. Diliberto, J. A. Near, R. M. Wightman, *J. Neurochem.* **1991**, *56*, 1855–1863; c) R. M. Wightman, J. A. Jankowski, R. T. Kennedy, K. T. Kawagoe, T. J. Schroeder, D. J. Leszczyszyn, J. A. Near, E. J. Diliberto, O. H. Viveros, *Proc. Natl. Acad. Sci. USA* **1991**, *88*, 10754–10758.

[13] a) S. T. Keene, C. Lubrano, S. Kazemzadeh, A. Melianas, Y. Tuchman, G. Polino, P. Scognamiglio, L. Cina, A. Salleo, Y. van de Burgt, F. Santoro, *Nat. Mater.* **2020**, *19*, 969–973; b) B. Zhang, M. L. Heien, M. F. Santillo, L. Mellander, A. G. Ewing, *Anal. Chem.* **2011**, *83*, 571–577.

[14] a) C. Amatore, A. I. Oleinick, I. Svir, *ChemPhysChem* **2010**, *11*, 149–158; b) F. Asadpour, X. Zhang, M. Mazloum-Ardakani, M. Mirzaei, S. Majdi, A. G. Ewing, *Chem. Sci.* **2021**, *12*, 10273–10278; c) X. Zhang, A. G. Ewing, *ACS Nano* **2022**, *16*, 9852–9858.

[15] M. T. Thompson, in *Intuitive Analog Circuit Design* (Ed.: M. T. Thompson), Newnes, Burlington, **2006**, pp. 13–42.

Manuscript received: July 28, 2022
Accepted manuscript online: September 8, 2022
Version of record online: September 29, 2022